

231702

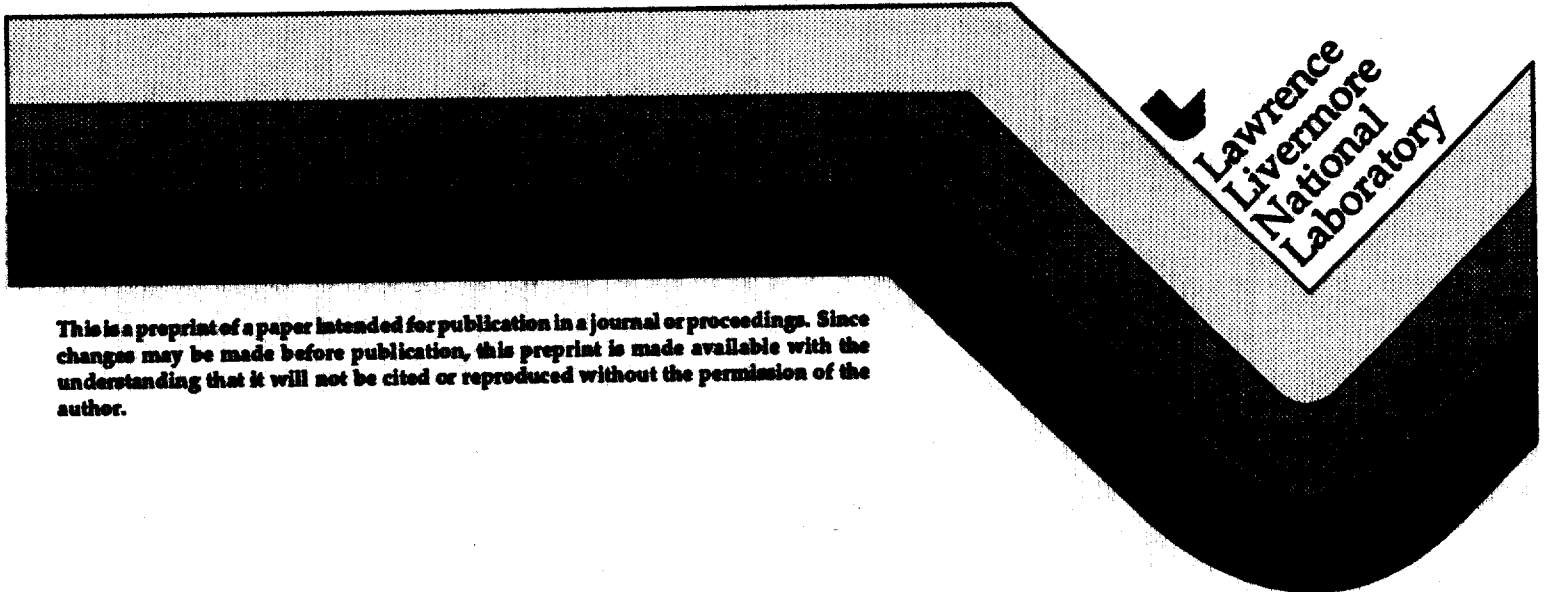
UCRL-JC-125100
PREPRINT

Experimental and Numerical Study of E-beam Evaporation of Titanium

**M. A. McClelland, K. W. Westerberg, T. C. Meier,
D. G. Braun, L. V. Berzins, T. M. Anklam, and J. Storer**

**This paper was prepared for submittal to the
Electron Beam Melting and Refining '96
Reno, Nevada
October 23-25, 1996**

November 26, 1996



The logo of Lawrence Livermore National Laboratory is a large, stylized 'L' shape. The top horizontal bar is light gray, and the vertical stem is dark gray. The right side of the 'L' is a white triangle pointing downwards, containing the text 'Lawrence Livermore National Laboratory' in black, stacked vertically. The bottom of the 'L' is a dark gray curve.

**Lawrence
Livermore
National
Laboratory**

This is a preprint of a paper intended for publication in a journal or proceedings. Since changes may be made before publication, this preprint is made available with the understanding that it will not be cited or reproduced without the permission of the author.

DISCLAIMER

This document was prepared as an account of work sponsored by an agency of the United States Government. Neither the United States Government nor the University of California nor any of their employees, makes any warranty, express or implied, or assumes any legal liability or responsibility for the accuracy, completeness, or usefulness of any information, apparatus, product, or process disclosed, or represents that its use would not infringe privately owned rights. Reference herein to any specific commercial product, process, or service by trade name, trademark, manufacturer, or otherwise, does not necessarily constitute or imply its endorsement, recommendation, or favoring by the United States Government or the University of California. The views and opinions of authors expressed herein do not necessarily state or reflect those of the United States Government or the University of California, and shall not be used for advertising or product endorsement purposes.

EXPERIMENTAL AND NUMERICAL STUDY OF E-BEAM EVAPORATION OF TITANIUM*

M. A. McClelland[†]
K. W. Westerberg
T. C. Meier
D. G. Braun
L. V. Berzins
T. M. Anklam

Lawrence Livermore National Laboratory
P.O. Box 808
Livermore, CA 94550 U.S.A.

J. Storer

3M
3M Center, Bldg. 60-1N01
Saint Paul, MN 55144 U.S.A.

Abstract

An experimental and numerical study is performed for the electron-beam evaporation of pure titanium from a bottom fed vapor source. In the experiments, an electron beam operating in the nominal range of 30-40 [kW] was used to evaporate metal from the top of a 3 [in] diameter rod. Variations were made in the e-beam power, sweep pattern, and sweep frequency, and the total evaporation rate was measured from feed consumption and laser absorption. The solid-pool interface was obtained from metallographic cross sections of the metal rod. A two-dimensional finite element model was developed for the melt which includes the effect of fluid flow and energy transport in the pool and conduction in the solid. The deformation of the liquid-vapor and solid-liquid interfaces are tracked using a mesh which stretches along spines parallel to the axis of the rod. For the cases considered, high evaporative fluxes and vapor pressures generate significant depressions in the top surface of the pool. Predicted and measured evaporation rates are in good agreement for moderate evaporation fluxes, but discrepancies are larger for the case involving the highest flux and deepest depression.

*Work performed under the auspices of the U. S. Department of Energy by the Lawrence Livermore National Laboratory under Contract W-7405-ENG-48. The authors wish to acknowledge the support of DARPA through the vapor phase manufacturing initiative (administered by Steve Wax) for supporting a portion of this work.

[†]Author to whom correspondence should be addressed.

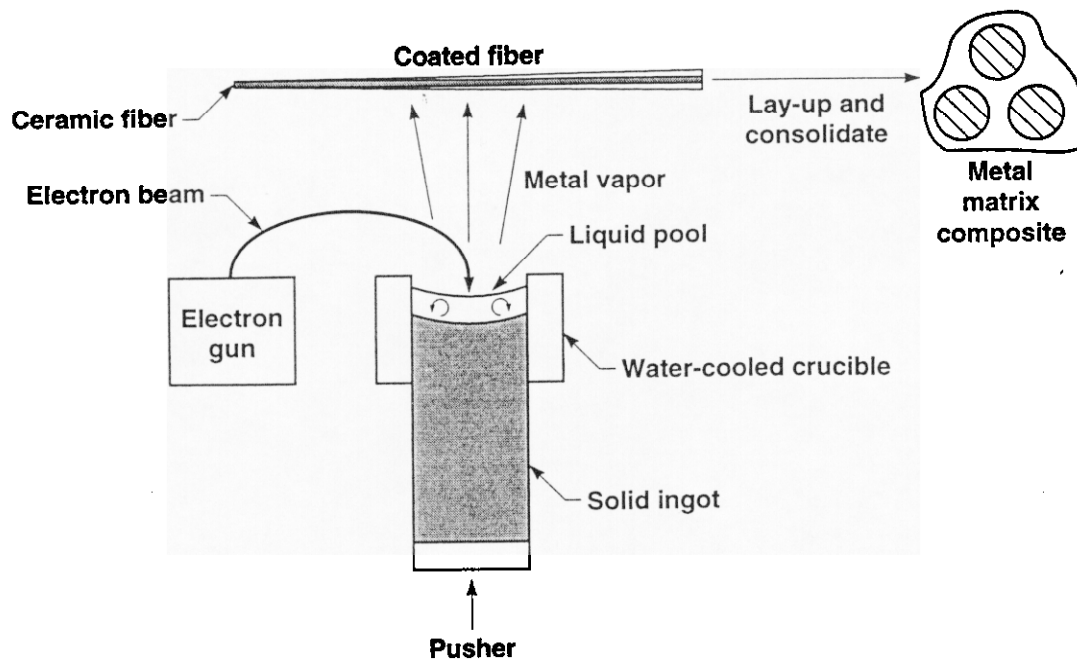


Figure 1: E-beam deposition of metal on fibers is an important step in the fabrication of metal matrix composites.

1 Introduction

The evaporation of Ti alloys is an important step in the manufacture of metal matrix composites for aircraft components [1]. In a typical process, the metal alloy is deposited on moving ceramic fibers using an electron-beam vapor source with bottom feed (see Figure 1). Process economics benefit from high vapor utilization and throughput while meeting specifications for coating thickness and composition. The characteristics of the vapor source play an important role in achieving these goals.

For the vapor source of Figure 1, an e-beam is used to heat the top of a rod which is advanced through a water-cooled crucible. Metal evaporates from the top of a pool which is confined by the crucible and the solid rod below. The liquid metal in the pool circulates strongly as a result of buoyancy and thermocapillary forces. At the beam impact site, the thrust of the departing vapor depresses the top surface of the liquid. These effects are strongly coupled and have a strong influence on performance.

Two practical situations illustrate the importance of these effects. In order to achieve high evaporation rates, the e-beam power is concentrated to achieve high temperatures and evaporation rates. However, if the vapor pressure is too high, the surface tension is insufficient to stabilize the surface. Metal droplets are ejected from the pool which can damage the fibers and coatings. Another challenge concerns the jamming of the feed rod which is influenced by the crucible geometry and the thermal expansion of the rod.

A detailed model of e-beam evaporation would assist in the design of the e-beam, crucible, and cooling systems. It would also help to select operating parameters such as e-beam power, sweep pattern, and sweep frequency which would potentially reduce the number of experiments needed to optimize the process.

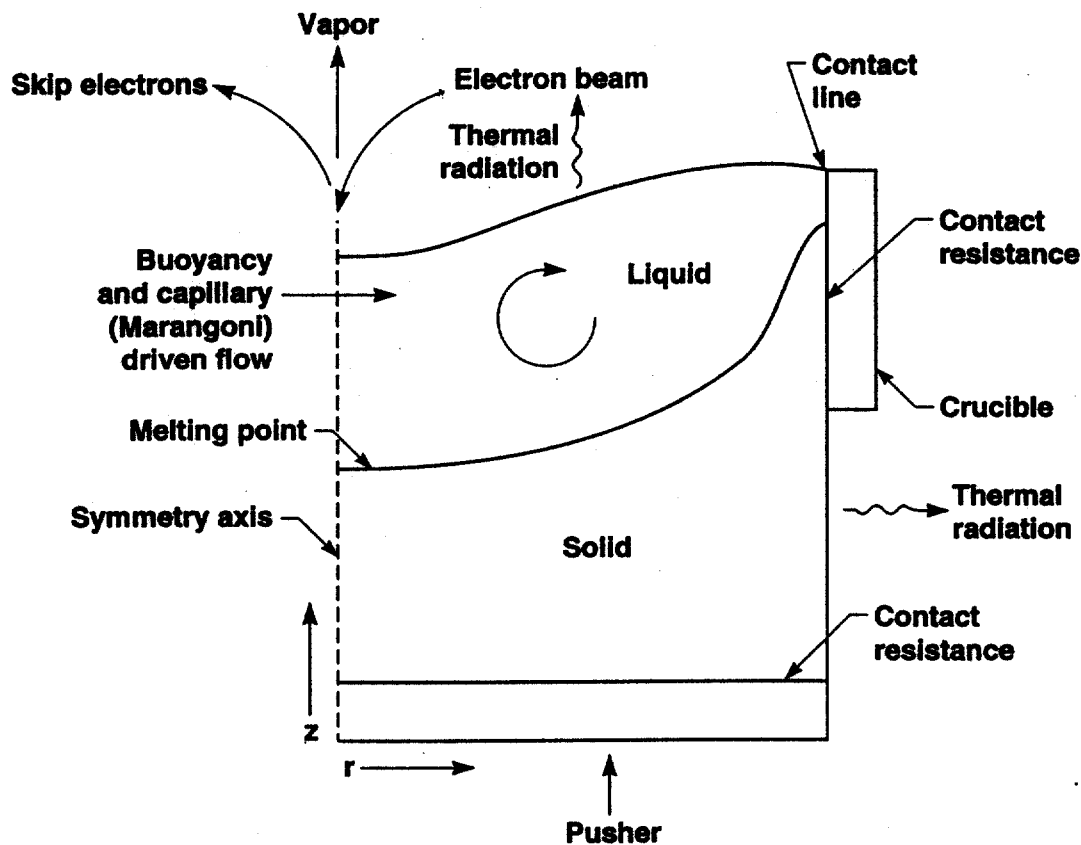


Figure 2: Model for bottom fed e-beam evaporation system.

Modeling of this e-beam evaporation system is a challenge due to the presence of moving phase boundaries including the liquid-vapor interface, the solid-liquid interface and the outer boundary of the ingot which expands with heating. In addition, buoyancy and thermocapillary forces generate intense flows in the transition region between laminar and turbulent flow.

Numerical models and methods have been developed for processes that share these same features such as crystal growth, welding, and casting systems. Many of these investigations are discussed elsewhere [2, 3]. We briefly mention two studies in which the mesh was deformed to track liquid-gas and solid-liquid interfaces. Sackinger *et al.* [4] employed the finite element method to analyze Czochralski crystal growth, and Lan and Kou [5] employed a control-volume finite difference method to model floating-zone crystal growth.

For the e-beam evaporation of cerium, Guilbaud [6] obtained results for a two-dimensional trough using a finite element method. The thermal and free surface profiles were calculated in a segregated fashion, and the results revealed the strong influence of a deep trench on evaporation rates.

Westerberg *et al.* [3, 7] developed two-dimensional planar and axisymmetric models for the steady e-beam evaporation from aluminum melts. Rotating spines were employed with a finite element method to track the horizontal position of the tri-junction and the locations of the solid-liquid and liquid-vapor interfaces. The results revealed the strong

interaction between fluid flow, thermal transport, and the deformation of free boundaries. In this work we apply the same approach to the e-beam evaporation of titanium from a bottom feed system. Model predictions for evaporation rate are compared with values measured from feed consumption and laser absorption.

2 Model Description

We present the important features of an e-beam evaporation model for bottom-fed titanium. The mathematical details for a similar steady-state evaporation system are given elsewhere [2, 3]. For the transient evaporation of metal from the top of a rod, we use a two-dimensional axisymmetric geometry. A single species is evaporated, and the model domain is divided into distinct vapor, liquid, and solid phase regions (see Figure 2). The vapor phase is treated with boundary conditions at the liquid-vapor interface as described below. The flow of liquid in the pool is governed by the Navier-Stokes equations with the Boussinesq approximation applied to the buoyancy term. The energy balance in the liquid phase includes accumulation, convection, and conduction terms. The convection term is excluded in the solid phase. Bulk material properties are treated as uniform in each of the liquid and solid phases, except for the buoyancy term.

A number of conditions for mass, momentum, and energy are applied at system boundaries. For steady-state cases, the average level of liquid in the pool is specified. The kinematic effects of evaporation on the flow field are neglected, and the vapor-liquid interface is treated as a material boundary. This is a good assumption since evaporation rates are generally small compared to the circulation rates in the pool.

The momentum balance at the liquid-vapor interface includes the normal force from surface tension as well as the tangential force generated by gradients in surface tension (Marangoni effect). For single species evaporation, the Marangoni effect is a surface shear stress resulting from temperature-induced gradients in the surface tension. This surface stress drives liquid from the beam impact area toward cold regions on the vapor-liquid interface. The momentum balance also includes the thrust from the departing vapor which is approximated as one-half of the vapor pressure. At the solid boundaries of the pool, the no-slip conditions are applied. Finally, the shear stress vanishes at the axis of symmetry.

Conditions are specified at the two endpoints of the liquid-vapor interface. At the axis of symmetry the interface is horizontal, and at the crucible wall the liquid height is specified. The latter condition provides an approximate representation of the fluid level near the crucible lip (see Figure 4). It is assumed that when the feed rate exceeds the evaporation rate, the liquid over flows on to the top of the crucible, and the liquid level in the cylinder of the crucible wall does not vary. A more detailed treatment would incorporate the overflow and resulting solidification.

At the beam impact site, the incident energy flux is described by a Gaussian distribution. The absorbed energy is taken to be a fixed fraction of the incident energy to account for the formation of skip electrons. At the liquid-vapor interface, a Stefan-Boltzmann (T^4) relationship describes losses due to thermal radiation. The latent heat loss includes the heat of vaporization and a translational contribution associated with vapor flow. The local evaporation flux is calculated using a Langmuir expression.

Heat flow from the liquid to the crucible wall is modeled with Newton's law of cooling using a single heat transfer coefficient to represent contact resistance. The heat loss from the solid material on the side of the ingot has contributions from crucible contact and

thermal radiation to the crucible and surroundings. The heat transfer coefficient associated with contact decreases linearly with temperature from the liquid value down to zero over a specified temperature range.

Thermal contact resistance between the ingot and pusher is also represented with a heat transfer coefficient. In order to minimize the effort associated with remeshing, the finite element domain is maintained at a length shorter than the metal ingot. The remaining lower portion of the ingot is modeled as a cooling fin, since the temperature field is nearly one-dimensional in this region. An effective heat transfer coefficient at the lower surface of the finite element domain accounts for the thermal behavior in the lower portion of the ingot.

The field equations and boundary conditions are discretized using a Galerkin finite element method. The mesh deforms along spines to track liquid-vapor and solid-liquid interfaces locations. The locations of the two interfaces are solved simultaneously with the flow and temperature fields using the Newton-Raphson method. A more complete discussion of the equations and the solution method is given elsewhere [3].

The MELT code can be used for both steady-state and time-dependent calculations. All results shown in this study are steady-state, but some were found by integrating from one steady-state to another using the false-transient method [8]. In this application, the backward Euler method was used with large time steps and error tolerances to damp strong solution transients and progress rapidly through the parameter space to the conditions of interest. This approach was particularly effective for traversing regions of the parameter space for which steady-state solutions were not available using traditional steady-state parameter continuation methods. [7, 9, 10].

3 Experimental System

An electron beam was used to evaporate bottom-fed titanium in the Evaporation Test Facility (ETF) at Lawrence Livermore National Lab. The ETF chamber has a side-mounted 100 [kW], e-beam gun which was operated at 30 [kV]. A beam spot is swept in circular patterns at 1 to 4 [kHz] to form rings. A pusher mechanism advances a 7.62 [cm] (3 [in]) diameter rod through a water-cooled crucible with a vertical wall height of 16.8 [cm].

Two video cameras provide views of the top surface of the melt pool. A high angle camera is used to position and monitor the electron beam. The view from a low angle camera is available to determine the pool level via an image processing scheme. For this approach, the pool is operated at a high level with the free surface bulging above the crucible lip. An edge detection method is used to measure the elevation of the vapor-liquid interface at a selected location. The top of the titanium rod occupies most of the camera view, giving high resolution (0.2 [mm/pixel]) and an interface elevation accurate to ± 0.5 [mm]. The feed rate for the rod is adjusted to keep the pool level near a setpoint value using a feedback control strategy involving Internal Model Control [11].

Evaporation rates are determined from feed consumption and laser absorption measurements. For the feed method, the linear advance of the rod is measured with the e-beam power, footprint, and pool level held constant. At the same time a laser beam tuned to an atomic transition in titanium is passed through the vapor plume. Using Beer's Law and a model for the vapor plume, the absorption can be converted to a vaporization rate [12, 13]. Parameters for the model were measured in previous experiments. Critical parameters include the vapor distribution, the vapor flow velocity, the electronic temperature and the

Table 1: Evaporation rates obtained during 5 experimental run periods.

Run Period	1	2	3	4	5
Description	base	high power	small ring	low freq.	base
Beam Power [kW]	33.3	39.3	33.3	33.3	33.3
Sweep freq. [kHz]	4.0	4.0	4.0	1.0	4.0
Feed rate [kg/h]	0.973	1.637	1.295	1.054	1.044
Laser vap. rate [kg/h]	1.10	1.78	1.64	1.28	1.26
Model vap. rate [kg/h]	1.35	2.00	2.23	1.35	1.35

transition strength.

4 Comparison of Numerical and Experimental Results

A series of five titanium evaporation experiments were conducted in which the total power, ring diameter, and sweep frequency were varied, and the evaporation rate was measured by feed consumption and laser absorption (see Table 1). Variations from the "base case" conditions (experiment no. 1) were made by adjusting each of the variables individually. In each experiment, the three independent variables and the pool level were held constant for a time interval in which nominally 2 [cm] (0.4 [kg]) of feed was consumed. At the end of the final experiment, which again involved base case conditions, the e-beam power was abruptly shut off to preserve the shape of the solid-liquid interface. It is noted that during the course of the experiments, some metal overflowed on to the top of the crucible as a result of operating the pool at a high level.

For the modeling of these experiments, several geometric and flow parameters must be specified. The average level of the pool above the crucible lip (0.42 [cm]) was taken from the metallographic cross section for the last run period. The contact line was measured to be 0.375 [cm] above the crucible lip. The Marangoni effect is assigned its full value associated with clean liquid metal. However, it is likely that contaminants reduced the temperature-sensitivity of the surface tension and the magnitude of the Marangoni effect. In order to resolve the strong flow and thermal convection using the meshes of this study, the viscosity was assigned a value twenty times the melting-point value given in Table 2. Although, it is likely that both the model Marangoni driving force and the viscous resistive force are higher than the physical forces, the comparison of results below suggests that their relative magnitudes are approximately correct. Other physical properties for titanium metal are given in Table 2.

There are also several thermal parameters which must be specified for the MELT model. The sweep frequency was taken to be high enough that the transient effects associated with the moving beam are negligible. This assumption is supported by the experimental results discussed below. The heat transfer coefficient selected for liquid-crucible contact (6000 [W/m²-K]) falls within the range of values measured for contact between liquid metal and metal molds [14]. It decreases linearly to zero as the temperature decreases 300 [°C] from the melting point. The heat transfer coefficient for the pusher (100 [W/m²-K]) also

Table 2: Physical properties of Ti metal.

Property	Value	Units
Melting point	1667	°C
Molecular weight	0.0479	kg/gmol
Liquid properties		
Viscosity	3.200×10^{-3}	kg/m-s
Density	4130	kg/m ³
Coeff. therm expansion	5.570×10^{-5}	K ⁻¹
Thermal conductivity	28.5	W/m-K
Heat capacity	8.129×10^2	J/kg-K
Surface tension	1.65	N/m
Surface tension (temp. deriv.)	-2.400×10^{-4}	N/m-K
Vapor pressure	$p_1 \exp(E/RT)$	N/m ²
p_1	2.317×10^{11}	N/m ²
E	-4.355×10^5	J/gmol
Heat of vaporization	9.092×10^6	J/kg
Thermal emissivity	$a_0 + a_1 T$	unitless
a_0	0.1810	unitless
a_1	2.533×10^{-5}	K ⁻¹
Skip fraction	0.29	unitless
Solid properties		
Density	4260	kg/m ³
Thermal conductivity	28.5	W/m-K
Heat capacity	8.129×10^2	J/kg-K
Thermal emissivity	0.4	unitless

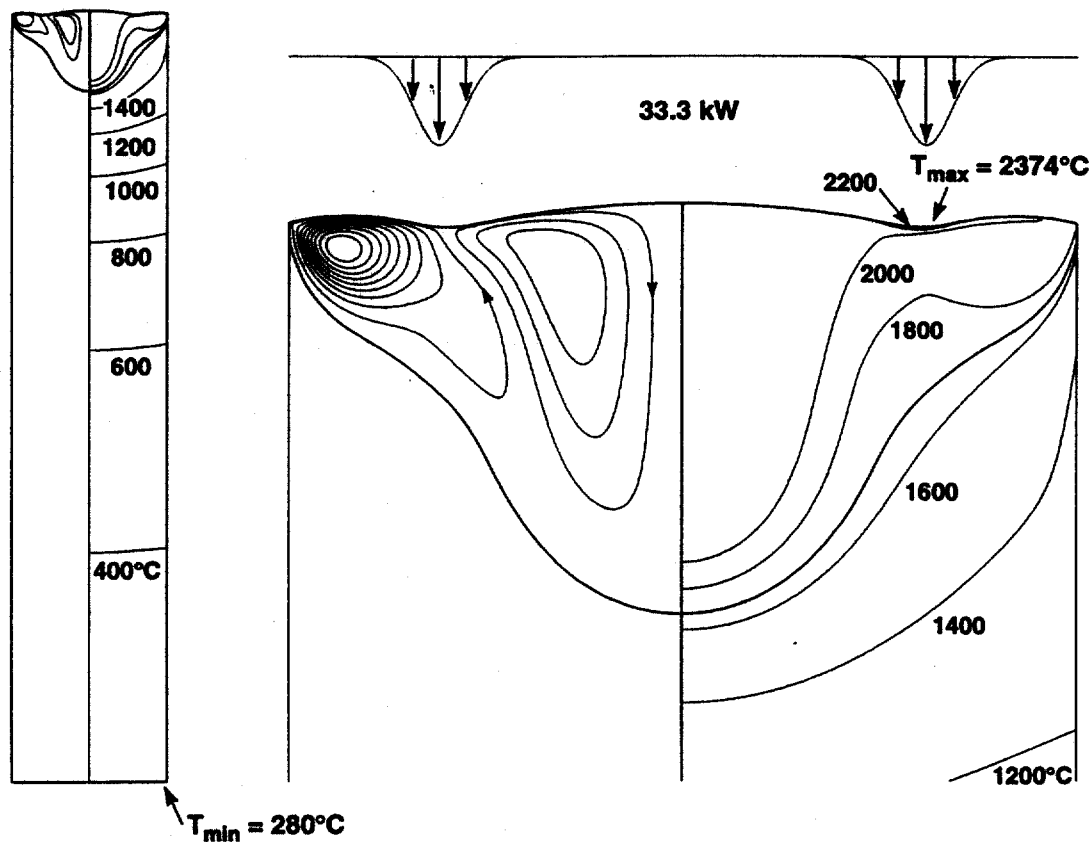


Figure 3: Pool shape, stream function and temperature countours for the large ring e-beam profile at 33.3 [kW].

is in the range of expected values for poor solid-solid contact. At the lower surface of the shortened finite element domain, an effective heat transfer coefficient ($83.4 \text{ [W/m}^2\text{-K]}$) is calculated using a cooling-fin model to account for the thermal effects of the remaining length of the rod.

For the base case (low power, large ring, high sweep frequency), predicted stream function, temperature contours, and interface locations are shown in Figure 3. At the beam impact site the recoil of the departing vapor forms a depression in the liquid-vapor interface which was observed with the low-angle camera during the experiment. There are two counter-rotating cells in the pool driven by buoyancy and capillary (Marangoni) forces. Liquid flows along the top pool surface from the hot beam impact area to the axis of symmetry and the cold crucible wall. The Marangoni effect creates very thin boundary layers in the flow field. The flow intensity is large based on a Reynolds number of 481 calculated using the maximum flow velocity (18.5 [cm/s]) and pool depth (4.02 [cm]) as characteristic values. The close spacing of the temperature contours at the beam impact location indicates that thermal convection is also strong ($Pe = 876$) and the thermal boundary layer is thin. Energy from the beam is swept strongly towards the cold wall and the center of the ingot where it forms a remarkably deep pool.

In Figure 4, the predicted pool boundary of Figure 3 is shown with the boundary

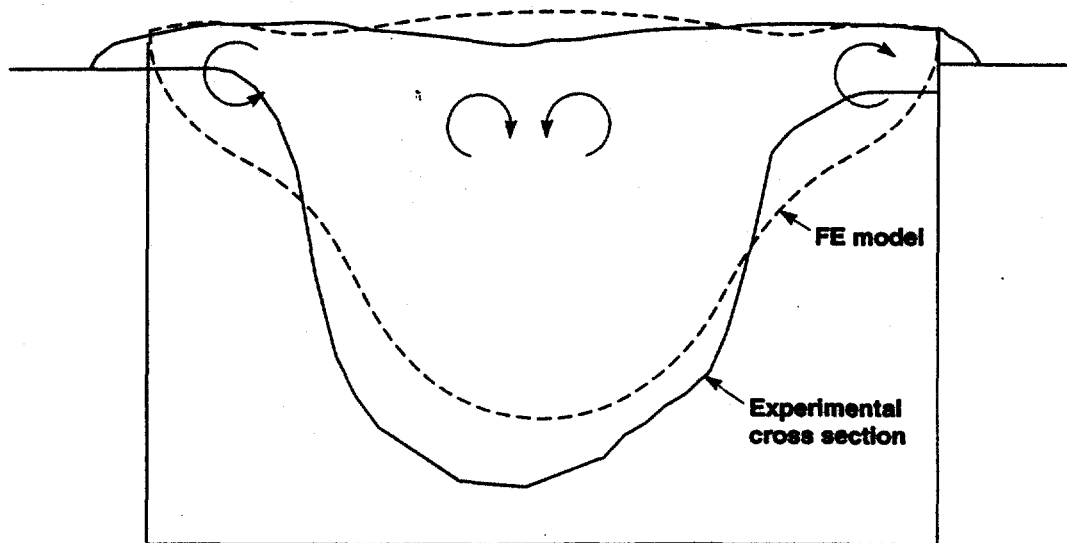


Figure 4: Comparison of the pool shape from the model to that obtained from a cross-section of a solidified rod for the large ring e-beam profile at 33.3 [kW]. Note that the liquid-vapor interface shape will be different due to solidification and cooling shrinkage of the rod.

measured from the ingot cross section. Useful comparisons can be made for the interface separating solid and liquid titanium, but not the overflow region or top surface of the pool. The overflow region is not part of the model domain, and the average level for the model top surface was set to match the measured profile as described in section 3. The trench in the pool disappears rapidly before solidification occurs and does not appear in the cross section. The model captures two important features of the solid-liquid interface which are the approximate depth of the pool and the inflection in the interface generated by the counter rotating cells. The large inward displacement of the measured melting line near the crucible lip suggests much better thermal contact than given by the model. A more detailed model could include a relatively low heat transfer coefficient in the overflow region and a high heat transfer coefficient between the liquid and the wall. However, the results below suggest that thermal details near the crucible wall do not strongly influence evaporation rates.

The evaporation rates of Table 1 show that the reduction in e-beam sweep rate from 4 to 1 [kHz] has a negligible effect. Consequently, the evaporation rates for the low sweep frequency were averaged with the base-case results. In addition, the base-case evaporation rates for the first and last run periods are in good agreement, suggesting that accumulated overflow material and the associated changes in the thermal contact had little effect. In Figure 5 the model, feed, and laser evaporation rates are plotted versus e-beam power for the two ring sizes. The e-beam power dependence for the model evaporation rate is nearly linear for both ring sizes. As the e-beam power increases the trench deepens while the circulation rate and latent heat loss increase. These factors reduce the rate of increase for the surface temperature and evaporation rate. For the large ring, the comparison between model and experimental values is very favorable with differences in evaporation rates less than 30%. The model values are the largest followed by the laser and feed values. It is

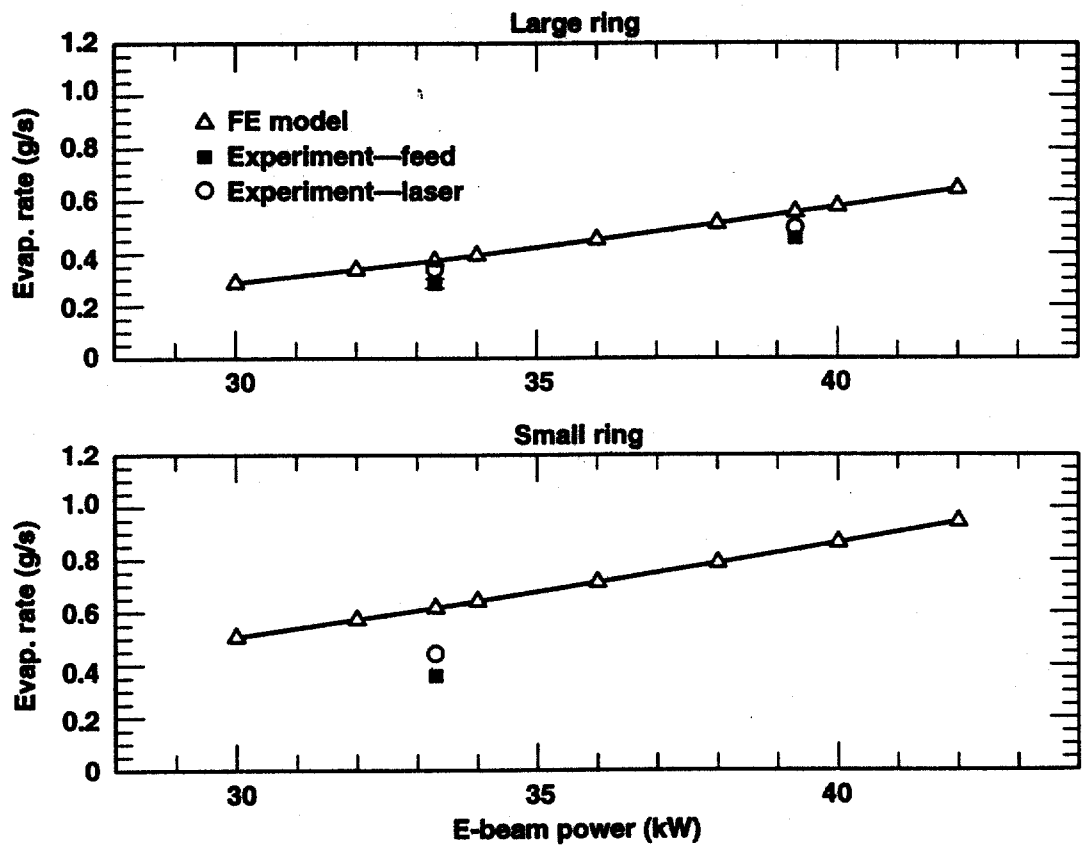


Figure 5: Model, feed and laser evaporation rates for large and small ring e-beam profiles as a function of power.

important to emphasize that the MELT model and laser absorption parameters were not adjusted to achieve this agreement. For the small ring, the discrepancies are larger which is attributed to the more severe conditions associated with the higher power density. The trench is deeper and the coupling between the liquid and vapor is more complex than given by the model.

5 Conclusions

A finite element model is developed for e-beam evaporation of pure Ti from a bottom fed vapor source. Model equations are discretized using a modified Galerkin finite element method where the mesh deforms along spines to track liquid-vapor and solid-liquid interface locations. The solution of the algebraic equations is obtained with a fully coupled Newton-Raphson method. Total evaporation rates are determined from feed consumption and laser absorption, and the shape of the solid-liquid interface is obtained from metallographic cross sections. A generally favorable comparison is achieved between model predictions and measurements suggesting that many of the important effects are correctly incorporated in the model.

References

- [1] J. Storer. Electron beam deposition for the fabrication of titanium MMCs. In R. Bakish, editor, *Electron Beam Melting and Refining State of the Art 1993*, pages 235–245. Bakish Materials Corp., Englewood, NJ, 1993.
- [2] K. W. Westerberg and M. A. McClelland. Modeling of material and energy flow in an EBCHR casting system. In R. Bakish, editor, *Electron Beam Melting and Refining State of the Art 1994*, pages 185–201. Bakish Materials Corp., Englewood, NJ, 1994.
- [3] K. W. Westerberg, M. A. McClelland, and B. A. Finlayson. Finite element analysis of flow, heat transfer, and free interfaces in an electron-beam vaporization system for metals. *submitted to Int. J. Numer. Methods Fluids*, 1997.
- [4] P. A. Sackinger, R. A. Brown, and J. J. Derby. A finite element method for the analysis of fluid flow, heat transfer and free interfaces in Czochralski crystal growth. *Int. J. Numer. Methods Fluids*, vol. 9, pp. 453–492, 1989.
- [5] G. W. Lan and S. Kou. Heat transfer, fluid flow and interface shapes in floating-zone crystal growth. *J. Crystal Growth*, vol. 108, pp. 351–366, 1991.
- [6] D. Guilbaud. Effect of melt surface depression on the vaporization rate of a metal heated by an electron-beam. In R. Bakish, editor, *Electron Beam Melting and Refining State of the Art 1995*, pages 227–242. Bakish Materials Corp., Englewood, NJ, 1995.
- [7] K. W. Westerberg, M. A. McClelland, and B. A. Finlayson. The interaction of flow, heat transfer, and free interfaces in an electron-beam vaporization system for metals. Paper 124e, 1994 Annual AIChE Meeting, San Francisco, CA, 1994.
- [8] P. M. Gresho, R. L. Lee, and R. L. Sani. On the time-dependent solution of the incompressible navier-stokes equations in two and three dimensions. In C. Taylor and K. Morgan, editors, *Recent advances in numerical methods in fluids*, volume 1, pages 27–79. Pineridge Press, Ltd., Swansea, U.K., 1980.
- [9] K. W. Westerberg, M. A. McClelland, and B. A. Finlayson. The tracking of interfaces in an electron-beam vaporizer. In R. W. Lewis, editor, *Numerical Methods in Thermal Problems*, volume VIII, Pt. 2, pages 1322–1333. Pineridge Press, Swansea, 1993.
- [10] K. W. Westerberg, M. A. McClelland, and B. A. Finlayson. Numerical simulation of material and energy flow in an e-beam melt furnace. In R. Bakish, editor, *Electron Beam Melting and Refining State of the Art 1993*, pages 153–165. Bakish Materials Corp., Englewood, NJ, 1993.
- [11] M. Morari and E. Zafiriou. *Robust process control*. Prentice Hall, 1989.
- [12] L. V. Berzins. Using laser absorption spectroscopy to monitor composition and physical properties of metal vapors. In *Chemical, Biochemical, and Environmental Fiber Sensors V, SPIE proceedings*, volume 2068, pages 28–40. 1993.
- [13] L. V. Berzins, T. M. Anklam, F. Chambers, S. Galanti, C. A. Haynam, and E. F. Worden. Laser absorption spectroscopy for process control — sensor system design methodology. *Surface and Coatings Technology*, vol. 76–77, pp. 675–680, 1995.

- [14] R. S. Ransing, Y. Zheng, and R. W. Lewis. Potential applications of intelligent pre-processing in the numerical simulation of castings. In R. W. Lewis, editor, *Numerical Methods in Thermal Problems*; volume VIII, Pt. 2, pages 361–375. Pineridge Press, Swansea, 1993.

Technical Information Department • Lawrence Livermore National Laboratory
University of California • Livermore, California 94551

